MAPAN-JOURNAL ,
Publisher: METROLOGY SOC INDIA , NPL PREMISES,
Address: DR K S KRISHNAN MARG, NEW DELHI, INDIA,
ISSN / eISSN:0970-3950 / 0974-9853
Volume 25-Issue 1-(2025)
https://doi-001.org/1025/17593913447904

OPEN ACCESS

Laser Raman Spectroscopy Analysis of Amitraz Pesticide

Xiaobin Wang

Check for updates

School of Physics and Electronic Information, Nanchang Normal University, Nanchang 330032, China

Corresponding author: tawangxiaobin@126.com

Funding：This study was supported by the Project Supported by National Natural Science Foundation of China (No. 32160417), and the Project Supported by Jiangxi Provincial Natural Science Foundation (20232BAB205026, 20242BAB20279).

Abstract

The Raman spectral signals of solid and liquid amitraz pesticides were collected by laser Raman spectrometer. The raw Raman spectral signals of amitraz solid were pre-processed with wavelet denoising, and the optimal parameter combinations for wavelet denoising were screened using orthogonal experimental design. Based on the vibrational modes of different functional groups, the denoised Raman spectra were segmented into three wavenumber regions (1800-1300 cm^{-1}, 1300-800 cm^{-1}, and 800-300 cm^{-1}). Peak assignment and analysis were conducted within each segment to elucidate the characteristic vibrational modes of the amitraz pesticide molecule across these spectral ranges. The results showed that the best denoising effect was achieved when using the ‘db4’ wavelet basis function, the number of decomposition layers was ‘2’, the thresholding scheme was ‘rigrsure’, and the retuning mode was ‘sln’, and the signal-to-noise ratio was 72.5502. In the Raman spectra of the amitraz pesticide, the intensity of the Raman peaks was higher at 719, 1243, 1399, 1606, and 1669 cm^{-1}, which can be used as the Raman characteristic peaks for the identification of amitraz pesticide. Raman peaks at 719 cm^{-1} and 1238 cm^{-1} were identified in the surface-enhanced Raman spectroscopy spectrum of the amitraz solution, which were basically consistent with the

characteristic peaks of amitraz powder pesticide. The results provide a basis for the determination of amitraz pesticide residues in food and agricultural products by laser Raman spectroscopy.

Keywords: Laser Raman spectroscopy; Amitraz pesticide; Wavelet denoising; Raman peak assignment

1. INTRODUCTION

Amitraz pesticide is a highly efficient and broad-spectrum insecticide and acaricide, which is mainly used for the control of mites in fruit trees, flowers, strawberries and other agricultural and horticultural crops, and is especially effective against mites in citrus fruits [1]. Under normal temperature and pressure conditions, amitraz exhibits relative chemical stability and resistance to decomposition. The amitraz solution exhibits significant irritant properties, affecting mucous membranes such as the oral cavity, eyes, and nasal passages, potentially inducing symptoms like coughing, rhinorrhea, conjunctival redness and swelling, and lacrimation upon exposure [2]. Furthermore, amitraz has a central nervous system depressant effect, necessitating strict regulation of dosage and exposure duration during application to mitigate neurotoxic risks [3]. Currently, analytical methodologies for the detection of amitraz pesticides primarily include gas chromatography-tandem mass spectrometry (GC-MS), liquid chromatography-mass spectrometry (LC-MS), and ultra performance liquid chromatography (UPLC) [4-6]. However, these techniques are characterized by limitations such as prolonged analysis duration, elevated operational costs, and complex sample preparation procedures.

Laser Raman spectroscopy is a spectroscopic analytical technique based on Raman scattering theory, capable of obtaining molecular vibrational and rotational information of substances. The position of Raman peaks indicates the presence of specific functional groups, making it a valuable

method for sample characterization and chemical analysis. Previous studies have employed Raman spectroscopy to analyze various pesticides [7]. Lian et al. [8] collected the Raman spectra of bifenthrin and employed density functional theory to analyze its vibrational modes, thereby identifying characteristic peaks for pesticide authentication. Ly et al. [9] investigated the surface-enhanced Raman scattering (SERS) spectra of fipronil pesticides. By analyzing the vibrational wavenumbers and Raman intensities of the theoretical Raman spectra of fipronil, they identified the characteristic peaks of its SERS spectrum. Gao et al. [10] conducted a theoretical analysis of the SERS spectra of the insecticide thiamethoxam, identifying the most intense Raman peak at 866 cm^{-1} as corresponding to the coupling of the N–N stretching vibrational mode and the symmetric N–O vibrational mode. Luca et al. [11] analyzed both conventional and SERS spectra of the organophosphorus pesticides dimethoate (DMT) and omethoate (OMT), elucidating differences in their Raman spectra through vibrational wavenumber and intensity analysis, and interpreting the vibrational modes associated with each Raman peak. These studies demonstrate that Raman spectral analysis of pesticide molecules can elucidate vibrational modes corresponding to characteristic peaks, facilitating pesticide identification. Currently, there are no reported studies on the Raman spectroscopic analysis of amitraz pesticides.

This study employed a laser Raman spectrometer to acquire Raman spectra of amitraz pesticide powders and solutions. Wavelet analysis was utilized to denoise the Raman spectra of the powder samples, thereby enhancing the signal-to-noise ratio of the spectral signals. The denoised spectra were segmented into three distinct spectral regions for peak assignment and analysis to identify characteristic Raman peaks. Based on the identified Raman characteristic peaks of amitraz, spectral

matching was performed to correlate these features with the Raman peaks observed in the SERS spectra of amitraz solutions.

2. MATERIALS AND METHODS

2.1 Instruments and Materials

A ZLRAM-1400 high-sensitivity laser Raman spectrometer (Zhonglang Zhengjian Biotechnology Co., Ltd., Suzhou, China) was employed, utilizing an excitation wavelength of 785 nm. The Raman spectral range was 200-2000 cm^{-1}, with a resolution of 2 cm^{-1}, an integration time of 10 seconds, and two accumulations. Amitraz pesticide (≥97%, Shanghai Aladdin Biochemical Technology Co., Ltd., Shanghai, China), acetonitrile (Xilong Chemical Co., Ltd., Shantou, China), and nano-enhancement reagents A and B (Zhonglang Zhengjian Biotechnology Co., Ltd., Suzhou, China) were used.

2.2 Raman Spectral Acquisition

For amitraz powder, an appropriate amount was placed on a glass slide and pressed flat to facilitate microscopic focusing, followed by spectral signal collection. To eliminate substrate interference, background scans of the glass slide were performed prior to measurement. For amitraz solutions, a concentration of 10 mg/L was prepared. In a 2 mL quartz vial, 500 μL of nano-enhancement reagent A, 20 μL of amitraz solution, and 100 μL of nano-enhancement reagent B were sequentially added, mixed thoroughly, and then transferred to the sample holder for spectral acquisition.

2.3 Spectral Preprocessing

During Raman spectral acquisition, factors such as laser source noise, external stray light, and CCD detector thermal noise introduce significant interference, resulting in noisy spectra that compromise the accuracy of peak position, intensity, and linewidth determination [12-14]. To accurately extract the spectral information of the analyte, raw Raman signals require preprocessing to minimize noise interference and enhance signal quality.

Currently, smoothing techniques are predominantly employed for spectral preprocessing. However, excessively large smoothing windows can diminish and broaden spectral features, while overly small windows may impair the smoothing effect. Additionally, smoothing can lead to the loss of fine spectral details [15]. Wavelet analysis, a time-frequency domain signal processing tool, offers advantages such as excellent localizability in both domains, flexible basis function selection, and decorrelation capabilities [16]. It enables multi-scale decomposition of spectral signals, isolating high-frequency noise components for effective noise removal. In this study, wavelet analysis was utilized to preprocess the Raman spectra of amitraz pesticide.

3. RESULTS AND ANALYSIS

3.1 Molecular structure and Raman spectra of amitraz

The molecular formula of amitraz is $C_{19}H_{23}N_3$, with its molecular structure depicted in Figure 1. As shown, the structure comprises phenyl, imino, and methyl groups, containing functional groups such as C–H, C=C, C–C–C, N–H, C–N, C=O, and $–CH_3$. Each functional group exhibits characteristic vibrational frequencies, enabling the assignment of Raman spectral peaks to identify the Raman characteristic peaks of amitraz pesticide [17].

The raw Raman spectrum of amitraz powder measured is presented in Figure 2. It is evident from the spectrum that the raw Raman signal contains significant noise. Prior to peak assignment and analysis of the amitraz Raman spectrum, preprocessing of the raw spectral data is necessary.

3.2 Wavelet denoising for Raman spectra of amitraz powder

When applying wavelet analysis for denoising Raman spectral signals, the parameters influencing the denoising efficacy include the type of wavelet basis, the number of decomposition levels, the thresholding scheme, and the reconstruction method. Appropriate selection of these parameters can achieve optimal denoising results. This study employed an orthogonal experimental design to identify the optimal combination of wavelet denoising parameters, using four factors as influencing variables and the signal-to-noise ratio (SNR) as the evaluation metric, conducting an L16 (2×4^3) mixed orthogonal experiment. The SNR refers to the ratio of the raw Raman spectral signal to the noise, calculated as follows:

$$SNR = 10 * \log\left(\sum_{i=1}^{n} f^2(i) / \sum_{i=1}^{n} \left(f(i) - \hat{f}(i)\right)^2\right)$$

where $f(i)$ is the raw Raman signal, $\hat{f}(i)$ is the Raman signal preprocessed by wavelet denoising.

Wavelet analysis involves numerous wavelet family functions, each comprising various basis functions. This study selects four commonly used wavelet basis functions: Haar, db4, sym8, and coif3 [18]. When the decomposition level exceeds five, the denoising effect shows no significant improvement. Therefore, decomposition levels of 2, 3, 4, and 5 are chosen [19]. The most commonly used threshold schemes for selection are Rigrsure (a software threshold estimator based on Stein's unbiased risk estimate), Sqtwolog (fixed threshold with a specified magnitude), Heursure (heuristic threshold selection combining the previous two methods), and Minimaxi (fixed threshold with an extremum minimizing mean square error) [20]. The reconstruction methods employed were sln

(which estimates noise at the first decomposition level to adjust the threshold) and mln (which estimates noise at each level for threshold adjustment) [21]. The design of the orthogonal experiment factors and levels is presented in Table 1, with results shown in Table 2. As can be seen from Table 2, factor C (decomposition level) has the greatest impact on the results, and the range of SNR values among the levels is 10.904. The influence hierarchy of the four factors on denoising results is C>B>D>A. Through comprehensive comparison, the optimal parameter combination was identified as $A_1B_2C_1D_1$, corresponding to the sln reconstruction method, db4 wavelet basis, 2 decomposition levels, and the Rigrsure thresholding scheme, achieving the highest SNR of 72.5502.

The raw spectral signal was denoised using a wavelet transform with the parameter combination $A_1B_2C_1D_1$. The denoised and reconstructed Raman spectrum is shown in Figure 3. Compared to the raw spectrum in Figure 2, the high-frequency noise components are significantly reduced in the denoised signal, and the Raman peaks are more prominent, facilitating peak attribution and spectral analysis.

To more clearly characterize the Raman spectral features of the amitraz pesticide molecule, the spectrum was divided into three wavenumber regions based on the vibrational modes of functional groups C=C, C–H, and C–C–C, and by referencing the Raman spectra of other substances containing identical functional groups and similar structures. These regions are 1300-1800 cm^{-1}, 800-1300 cm^{-1}, and 300-800 cm^{-1} for peak assignment and analysis.

3.3 Raman spectra of amitraz at 1300-1800 cm^{-1}

The Raman spectrum of amitraz in the range of 1300-1800 cm^{-1} is shown in Figure 4. It can be seen from the figure that the number of Raman peaks of amitraz pesticide in this wavenumber range is relatively small. Except 1574 cm^{-1} and 1375 cm^{-1}, the intensity of other spectral peaks was higher,

which were located at 1669, 1606, 1493 and 1399 cm^{-1}, respectively. The Raman peaks within this wavenumber range are mainly caused by C=N stretching vibrations and C–C stretching vibrations.

(1) The stretching vibration of C=N in the RCH=NR' group is within the range of 1675-1665 cm^{-1} [22], and this spectral band can be found at 1669 cm^{-1}.

(2) In spectra of benzene derivatives, four C–C stretching vibration bands are observed near 1600, 1580, 1500, and 1450 cm^{-1} within the 1630-1450 cm^{-1} range [23]. The first band typically appears concurrently with the second, both manifesting as strong bands in the Raman spectrum. Two Raman peaks can be found at 1606 and 1574 cm^{-1} in the figure, which are double peaks. Under normal circumstances, the third spectral band near 1500 cm^{-1} is less conspicuous in the Raman spectrum, often obscured by the antisymmetric deformation of methyl groups on the aromatic ring. This spectral band is observed at 1493 cm^{-1}, which is the coupling of C–C stretching vibration and CH_3 antisymmetric deformation vibration in benzene ring.

(3) Additional peaks include the band at 1399 cm^{-1}, attributed to in-plane C–H bending vibrations of the methylene group, and the band at 1375 cm^{-1}, associated with symmetric deformation vibrations of methyl groups in amitraz.

3.4 Raman spectra of amitraz at 800-1300 cm^{-1}

The Raman spectrum of amitraz in the range of 800-1300 cm^{-1} is shown in Figure 5. Within this wavenumber range, the Raman spectrum of amitraz have more peaks, and only 1243 cm^{-1} and 958 cm^{-1} have higher intensities. It is mainly caused by C–H in-plane deformation vibration, C–H out of plane swing vibration and the stretching vibration of the skeleton of the benzene ring.

(1) The in-plane deformation vibration of C–H has a series of very strong sharp spectral bands in the range of 1300-960 cm^{-1}, which can confirm the existence of aromatic rings [24]. In the Raman spectrum of amitraz, it can be found at 1281, 1155, 1120 cm^{-1}.

(2) The skeletal stretching vibration of 1,2,4 - trisubstituted benzene is located at 1280-1200 cm^{-1} [25]. This spectral band can be found at 1243,1223 and 1201 cm^{-1} in the figure.

(3) The bands at 958, 944, and 931 cm^{-1} are attributed to out-of-plane C–H wagging vibrations of the secondary methyl groups. Specifically, the 958 cm^{-1} band results from synchronized out-of-plane wagging of C–H bonds in both methyl groups, while the 944 cm^{-1} and 931 cm^{-1} bands arise from cross out-of-plane wagging modes of the C–H bonds in the methyl groups.

(4) The position of the C–H out-of-plane bending vibration spectral band depends on the number of hydrogen atoms connected to the ring. When the number of hydrogen atoms is 3, the spectral band is located at 810-750 cm^{-1} [26]. It can be found at 808 cm^{-1} in the figure.

(5) Additional spectral peaks include a band at 903 cm^{-1}, assigned to the C–N stretching vibration in methylamine, and a band at 867 cm^{-1}, corresponding to the antisymmetric deformation vibration of the methyl groups in methylamine.

3.5 Raman spectra of amitraz at 300-800 cm^{-1}

The Raman spectrum of amitraz in the range of 300-800 cm^{-1} is shown in Figure 6. In this wavenumber range, all peaks except at 719 cm^{-1} exhibit relatively weak intensities, primarily attributable to vibrations of the whole framework of amitraz. However, the vibrational modes of specific functional groups dominate the peak positions, predominantly arising from the breathing and out-of-plane bending modes of the phenyl rings.

(1) One of the strongest spectral bands (polarized) in the Raman spectrum of 1,2,4-trisubstituted benzene occurs in the range of 750-150 cm^{-1} [25]. This spectral band can be found at 719 cm^{-1}, which is the peak intensity of this band and belongs to the respiratory vibration of two benzene rings.

(2) Other characteristic Raman bands of 1,2,4-trisubstituted benzene are located at 580-540 cm^{-1} (variable intensity) and 500-450 cm^{-1} (variable intensity) [25]. It can be found at 565, 538 and 500 cm^{-1} in the figure, which is mainly caused by the skeleton stretching vibration of two benzene rings, among which 565 cm^{-1} and 538cm^{-1} are double peaks.

(3) The Raman peaks of 596, 463 and 443 cm^{-1} are mainly caused by the out-of-plane bending vibration of the two benzene rings, among which 463 cm^{-1} and 443 cm^{-1} are double peaks.

(4) The Raman peaks at 349 cm^{-1} and 322 cm^{-1} are primarily associated with C–H out-of-plane wagging vibrations of the secondary methyl groups, also presenting as a doublet.

(5) Other Raman peaks: 399 cm^{-1} is mainly caused by the out-of-plane bending vibration of C–N–C in the middle of the entire skeleton. 384 cm^{-1} is mainly caused by the torsional vibration of two benzene rings.

3.6 Raman characteristic peaks of amitraz pesticide

By assigning and analyzing the Raman spectral peaks of the amitraz pesticide, the characteristic vibrational modes of the molecule were identified. There are five spectral peaks with relatively high intensity at 719, 1243, 1399, 1606 and 1669 cm^{-1}, which can be used as the Raman characteristic peaks of the amitraz pesticide. The SERS spectrum of the amitraz pesticide (with a concentration of 10 mg/L) is shown in Figure 7. It can be seen from the figure that the Raman peaks

are obvious at 719 cm^{-1} and 1238 cm^{-1}, and their positions are basically consistent with the Raman characteristic peaks of amitraz powder.

4. CONCLUSION

This study employs wavelet denoising method to preprocess the raw Raman signals of solid amitraz pesticide, utilizing a hybrid orthogonal design to optimize the parameters for wavelet denoising. The results demonstrate that the wavelet denoising method effectively removes the majority of noise from the raw Raman spectra. The Raman spectra of the denoted amitraz pesticide powder were subjected to peak attribution and analysis to obtain its characteristic vibration modes, and its Raman characteristic peaks were identified. The Raman characteristic peaks of the solid amitraz pesticide are basically consistent with those of the liquid, which can be used as the basis for qualitative discrimination of amitraz pesticide residues in food and agricultural products.

Ethical Compliance

There are no researches conducted on animals or humans.

Conflict of Interests

There are no conflicts to declare.

Acknowledgment

This study was supported by the Project Supported by National Natural Science Foundation of China (No. 32160417), and the Project Supported by Jiangxi Provincial Natural Science Foundation (20232BAB205026, 20242BAB20279).

References

[1] Yu S. J., Cong L., Liu H. Q., Ran C. Genetic analysis and screening of detoxification-related genes in an amitraz-resistant strain of Panonychus citri. Bulletin of Entomological Research, 2020, 10(6): 743-755. DOI: 10.1017/S0007485320000267.

[2] Dhooria S., Agarwal R. Amitraz, an underrecognized poison: A systematic review. Indian Journal of Medical Research, 2016, 144: 348-358. DOI: 10.4103/0971-5916.198723.

[3] Herath H. M. M. T. B., Pahalagamage S. P., Yogendranathan N., Wijayabandara M. D. M. S., Kulatunga A. Amitraz poisoning: A case report of an unusual pesticide poisoning in Sri Lanka and literature review. BMC Pharmacology & Toxicology. 2017, 18: 6(1)-6(6). DOI: 10.1186/s40360-016-0114-5

[4] Özcan N., Akman S. Determination of amitraz and its degradation products and monitoring degradation process in quince and cucumber. International Journal of Environmental Analytical Chemistry. 2019, 99(4): 357-368. DOI: 10.1080/03067319.2019.1596266.

[5] Gao X., Sun Y. B., You H. D., Dai Y. N., Guo H., Zhao Q. B. Simultaneous determination of amitraz, chlordimeform, formetanate and metabolites in human blood by liquid chromatography tandem mass spectrometry with phospholipid-removal pretreatment. Biomedical Chromatography. 2019, 33(4): e4477(1)-e4477(9). DOI10.1002/bmc.4477.

[6] Li Y. P., Li Y. X., Yang Y. Rapid screening of amitraz and its metabolite residues in honey using a quick, easy, cheap, effective, rugged, and safe extraction method coupled with UHPLC and Q Exactive. Journal of Separation Science. 2020, 43(8): 1466-1473. DOI: 10.1002/jssc.201900801.

[7] Schneider H., Hebel J., Böhm B., Kneer R., Dreizler A. Rotational-vibrational O_2-CO_2 coherent anti-Stokes Raman spectroscopy for determination of thermochemical states in oxy-fuel biomass combustion. Proceedings of the Combustion Institute. 2024, 40(1-4): 105457(1)-105457(7). DOI10.1016/j.proci.2024.105457.

[8] Lian S., Chen B., Gu Y. F., Song C., Lei J. J., Gao X. The Study of Raman Spectroscopy of Bifenthrin Molecular. Spectroscopy and Spectral Analysis. 2020, 40(6): 1952-1955. DOI: 10.3964/j.issn.1000-0593(2020)06-1952-04.

[9] Ly N. H., Nguyen T. H., Nghi N. D., Kim Y. H., Joo S. W. Surface-Enhanced Raman Scattering Detection of Fipronil Pesticide Adsorbed on Silver Nanoparticles. Sensors. 2019, 19(6): 1355(1)-1355(10). DOI: 10.3390/s19061355.

[10] Gao Y., Xu M. L., Xiong J. F. Raman and SERS spectra of thiamethoxam and the Ag_3-thiamethoxam complex: an experimental and theoretical investigation. Journal of Environmental Science and Health Part B - Pesticides Food Contaminants and Agricultural Wastes. 2019, 54(8): 665-675. DOI: 10.1080/03601234.2019.1631099.

[11] Guerrini L., Sanchez-Cortes S., Cruz V. L., Martinez S., Ristori S., Feis A. Surface-enhanced Raman spectra of dimethoate and omethoate. Journal of Raman Spectroscopy. 2011, 42(5): 980-985. DOI: 10.1002/jrs.2823.

[12] Fang S. Y., Wu S. Y., Chen Z., He C., Li Lin L., Ye J. Recent progress and applications of Raman spectrum denoising algorithms in chemical and biological analyses: A review. Trac-Trends in Analytical Chemistry. 2024, 172: 117578(1)-117578(18). DOI: 10.1016/j.trac.2024.117578.

[13] Goedhart J. J., Kuipers T. P., Papadakis V. M. Raman and photoluminescence signal separation in Raman hyperspectral imagery including noise reduction. Journal of Raman Spectroscopy. 2024, 55(5): 598-614. DOI: 10.1002/jrs.6651.

[14] Iqbal M. A., Tan M., Krzczanowicz L., El-Taher A. E., Forysiak W., Ania-Castañón J. D., Harper P. Noise and transmission performance improvement of broadband distributed Raman amplifier using bidirectional Raman pumping with dual order co-pumps. Optics Express. 2017, 25(22): 27533-27542. DOI: 10.1364/OE.25.027533.

[15] Kang N., Liu H. Y., Zhou S. L., Zhao Y., Lei A. L. Inhibition of stimulated Raman side-scattering with one-dimensional smoothing by spectral dispersion. Journal of the Optical Society of America B - Optical Physics. 2021, 38(12): 3567-3574. DOI: 10.1364/JOSAB.435784.

[16] Sharan T. S., Sharma S., Sharma N. Denoising and Spike Removal from Raman Spectra using Double Density Dual-Tree Complex Wavelet Transform. Journal of Applied Spectroscopy. 2021, 88(1): 117-124. DOI: 10.1007/s10812-021-01149-9.

[17] Lu Y., Wu L. W., Cao W. M., Huang Y. F. Finding a Sensitive Surface-Enhanced Raman Spectroscopic Thermometer at the Nanoscale by Examining the Functional Groups. Analytical Chemistry. 2022, 94(15): 6011-6016. DOI: 10.1021/acs.analchem.2c00633.

[18] Ismael A., A. Baykara M. Image Denoising Based on Implementing Threshold Techniques in Multi-Resolution Wavelet Domain and Spatial Domain Filters. Traitement du Signal. 2022, 39(4): 1119-1131. DOI: 10.18280/ts.390404.

[19] Bekerman W., Srivastava M. Determining Decomposition Levels for Wavelet Denoising Using Sparsity Plot. IEEE Access. 2021, 9: 110582-110591. DOI: 10.1109/ACCESS.2021.3103497.

[20] Zhou H. X., Wang X. Y., Zhong S. J., Li Y. B., Xi K. W. Multipath error extraction and mitigation based on refined wavelet level and threshold selection. GPS Solutions. 2024, 28(4): 157(1)-157(18). DOI: 10.1007/s10291-024-01704-9.

[21] Ong P. M., Galvez M. C., Vallar E., Shiina T. Wavelet Denoising Applied to Light Emitting Diode Lidar Signal. Advanced Science Letters. 2017, 23(2): 1374-1378. DOI: 10.1166/asl.2017.8352.

[22] Suda K., Yokogawa D. Theoretical Understanding of the Nonlinear Raman Shift of C-N Stretching Vibration of p-Aminobenzonitrile in Supercritical Water. Journal of Physical Chemistry B. 2023, 127(13): 3010-3015. DOI: 10.1021/acs.jpcb.2c09034.

[23] Ren P. P., Men Z., Wang S. H., Sun C. L. Coupling competition and energy transfer between C=C and C-H vibration in the process of cascaded stimulated Raman scattering of benzene-methanol solution. Applied Physics Letters. 2024, 125(4): 041102(1)-041102(8). DOI: 10.1063/5.0218457.

[24] Dong X. H., Yang F. W., Yu H., Yao W. R., Xie Y. F. Rapid Detection of Zilpaterol Residues in Pork by Surface-Enhanced Raman Spectroscopy. Spectroscopy and Spectral Analysis. 2022, 42(9): 2843-2847. DOI: 10.3964/j.issn.1000-0593(2022)09-2843-05.

[25] Ferger M., Ban Z., Krosl I., Tomic S., Dietrich L., Lorenzen S., Rauch F., Sieh D., Friedrich A., Griesbeck S. Bis(phenylethynyl)arene Linkers in Tetracationic Bis-triarylborane Chromophores Control Fluorimetric and Raman Sensing of Various DNAs and RNAs. Chemistry - A European Journal. 2021, 27(16): 5142-5159. DOI: 10.1002/chem.202005141.

[26] Ullah N., Jiao Z. R., Bai J. L., Wang Z. Q., Zhang R. T., Ma L., Lin K. Removing Fermi resonance through deuterated molecules with single C-H bond in C-H stretching region of Raman spectra. Chinese Journal of Chemical Physics. 2024, 37(6): 783-791. DOI: 10.1063/1674-0068/cjcp2408117.

Table 1. Design of orthogonal experiment factors and levels for wavelet denoising.

NO.	Reconstruction method (A)	Wavelet basis function (B)	Decomposition level (C)	Threshold scheme (D)
1	sln	haar	2	Rigrsure
2	mln	db4	3	Sqtwolog
3	sln	sym8	4	Heursure
4	mln	coif3	5	Minimaxi

Table 2. Orthogonal experimental results of wavelet denoising.

NO.	A	B	C	D
1	57.752	51.538	61.269	57.882
2	52.001	58.784	56.849	51.363
3	58.474	55.713	54.169	56.777
4	54.425	56.617	50.365	56.630
Range	6.473	7.246	10.904	6.519
Optimal	A_1	B_2	C_1	D_1

Captions

Figure 1 Molecular structure of amitraz.

Figure 2 Raw Raman spectra of amitraz powder.

Figure 3 Raman spectra of amitraz powder preprocessed by wavelet denoising.

Figure 4 Raman spectra of amitraz at 1300-1800 cm^{-1}.

Figure 5 Raman spectra of amitraz at 800-1300 cm^{-1}.

Figure 6 Raman spectra of amitraz at 300-800 cm^{-1}.

Figure 7 SERS spectra of amitraz solution (10mg/L).

Figure 1

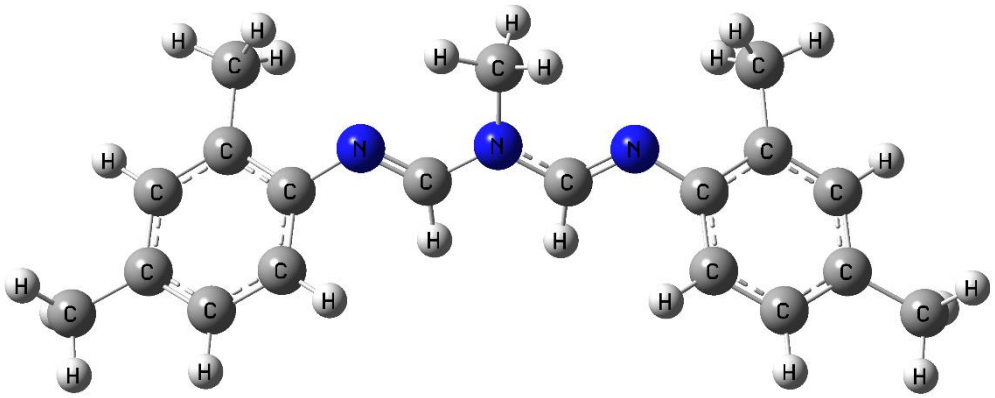

Figure 1 Molecular structure of amitraz.

Figure 2

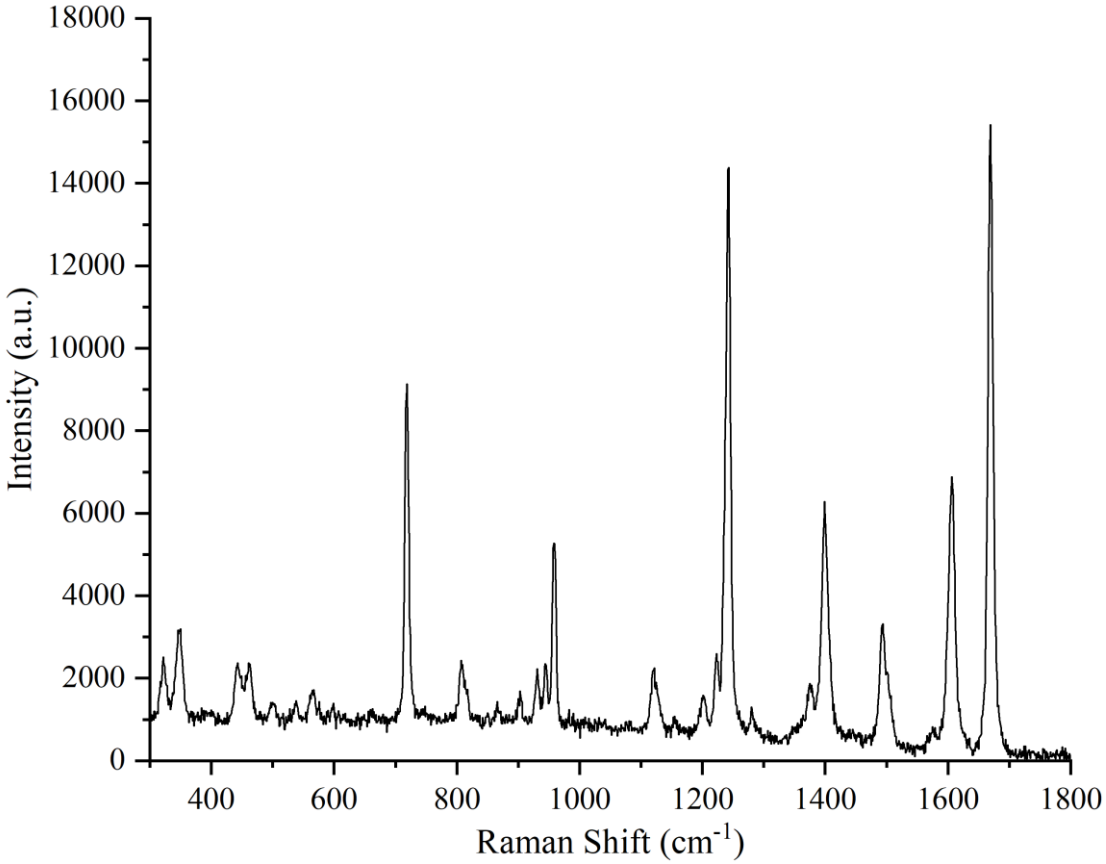

Figure 2 Raw Raman spectra of amitraz powder.

Figure 3

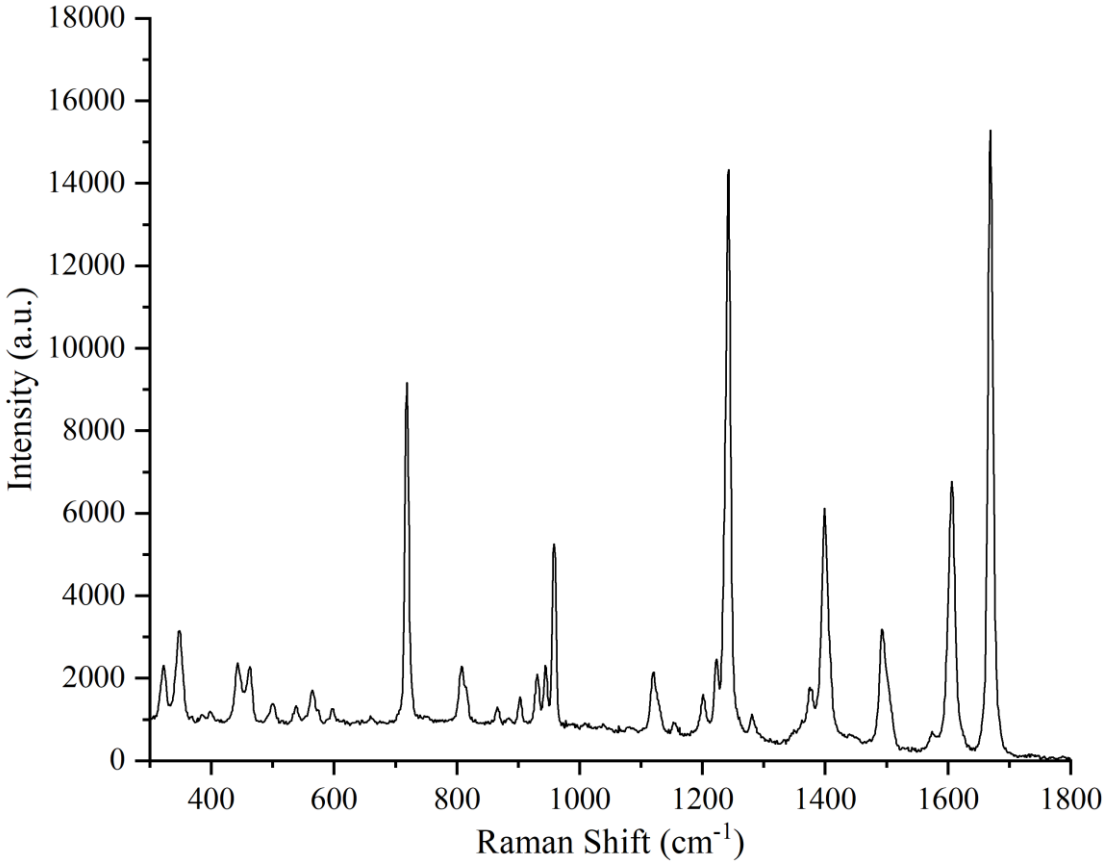

Figure 3 Raman spectra of amitraz powder preprocessed by wavelet denoising.

Figure 4

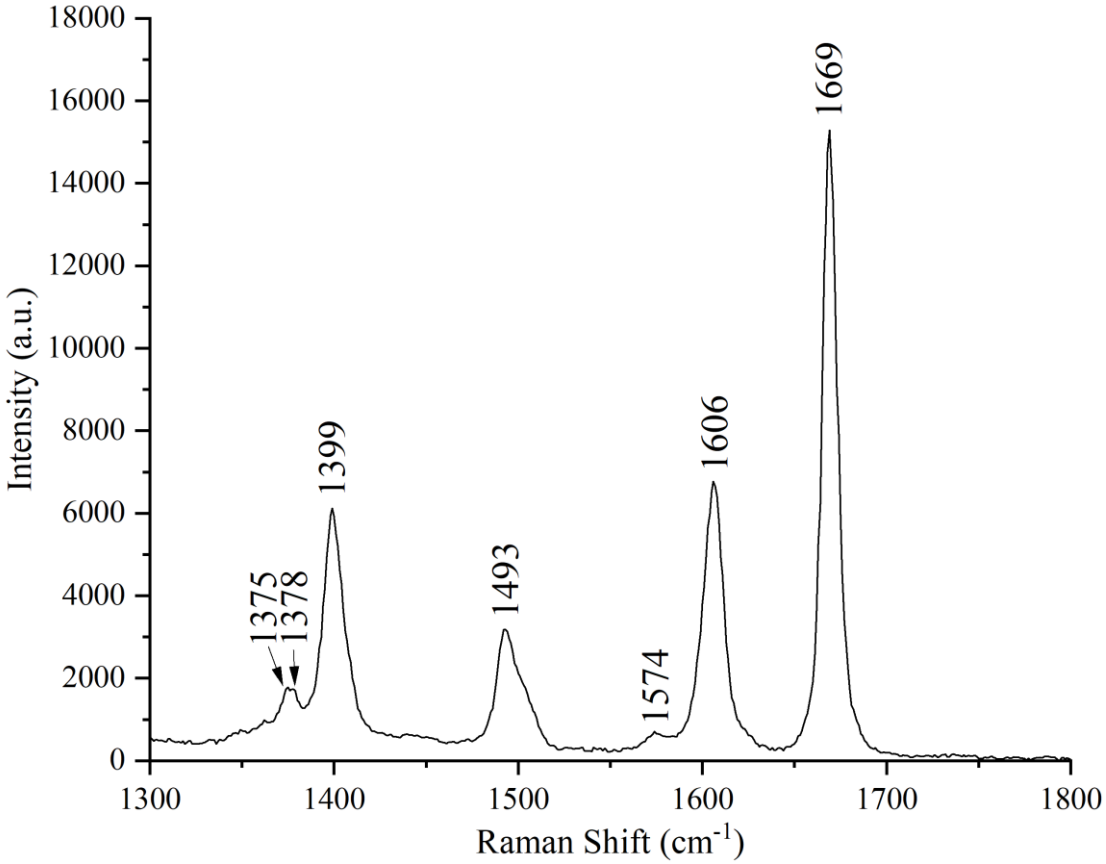

Figure 4 Raman spectra of amitraz at 1300-1800 cm^{-1}.

Figure 5

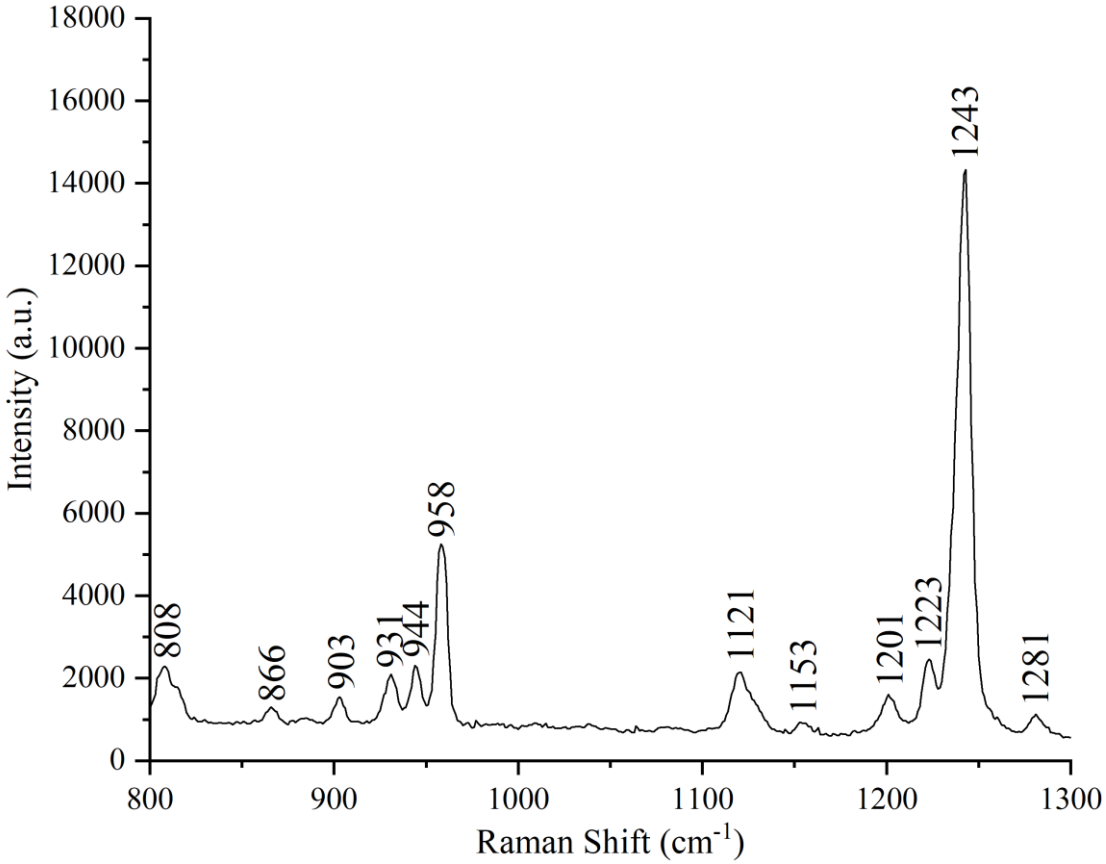

Figure 5 Raman spectra of amitraz at 800-1300 cm^{-1}.

Figure 6

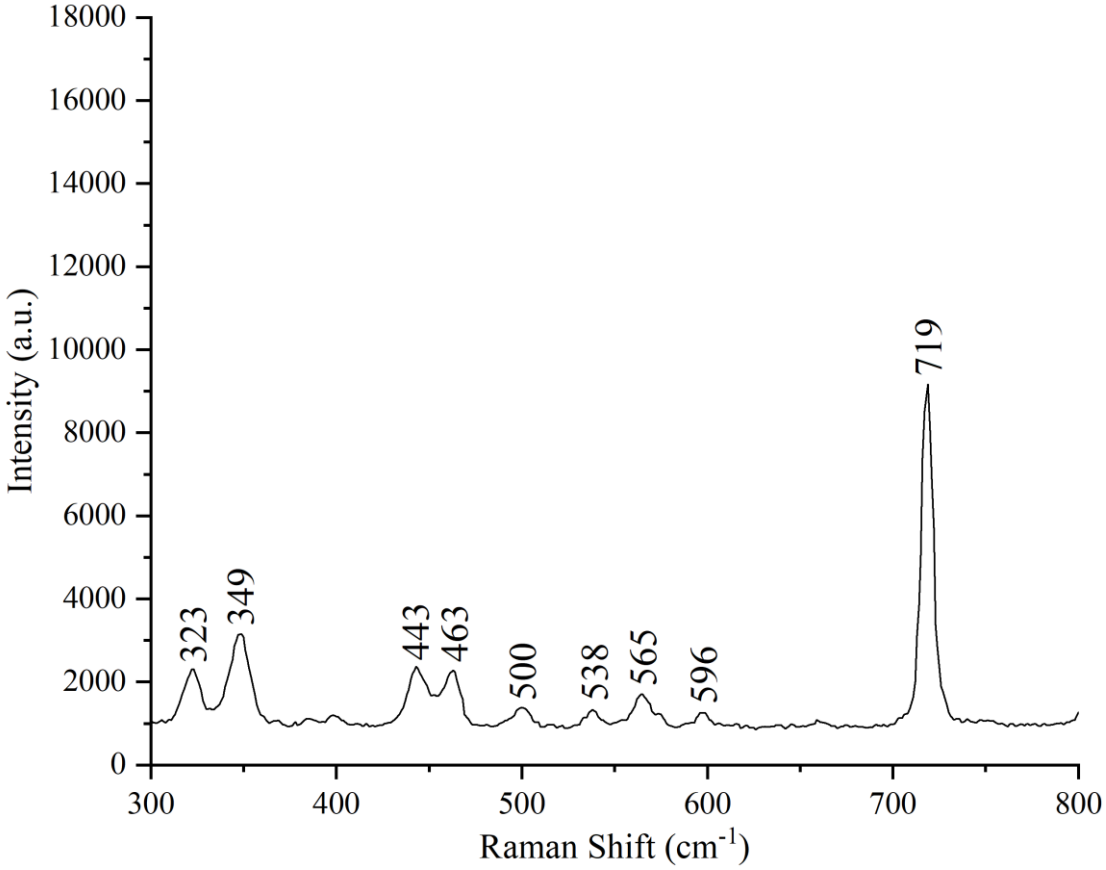

Figure 6 Raman spectra of amitraz at 300-800 cm^{-1}.

Figure 7

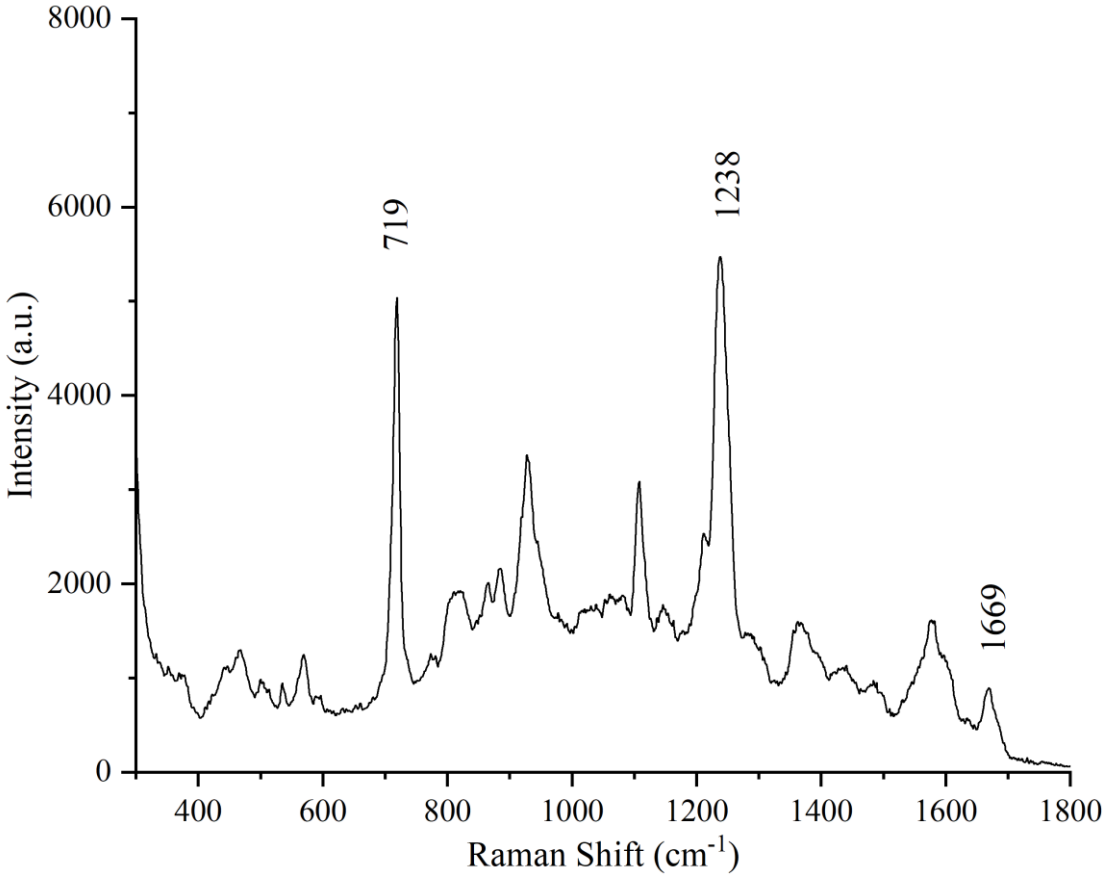

Figure 7 SERS spectra of amitraz solution (10mg/L).